



# Low Young's Modulus TiNbSn Alloy Locking Plates Accelerate Osteosynthesis in Rabbit Tibiae

Masashi Koguchi,<sup>1</sup> Yu Mori,<sup>1</sup> Masayuki Kamimura,<sup>1</sup> Kentaro Ito,<sup>1</sup>  
Hidetatsu Tanaka,<sup>1</sup> Hiroaki Kurishima,<sup>1</sup> Tomoki Koyama,<sup>1</sup> Naoko Mori,<sup>2</sup>  
Naoya Masahashi<sup>3</sup> and Toshimi Aizawa<sup>1</sup>

<sup>1</sup>Department of Orthopaedic Surgery, Tohoku University Graduate School of Medicine, Sendai, Miyagi, Japan

<sup>2</sup>Department of Radiology, Akita University Graduate School of Medicine, Akita, Akita, Japan

<sup>3</sup>Institute for Material Research, Tohoku University, Sendai, Miyagi, Japan

A new beta TiNbSn alloy with a low Young's modulus of approximately 40 GPa has been developed to resolve the stress shielding by Young's modulus divergence. In this study, the efficacy of TiNbSn alloy locking plates on bone repair is compared to that of commercially pure titanium (CP-Ti). The TiNbSn alloy and CP-Ti, which have Young's moduli of 49.1 GPa and 107 GPa, respectively, were compared. Male Japanese white rabbits were anesthetized, and osteotomy and osteosynthesis with locking plates were performed on the right tibia. The bone repair was assessed using micro-computed tomography (CT), histomorphometry, immunohistochemistry, and mechanical testing. Micro-CT, histomorphometry, immunohistochemistry, and mechanical testing were performed four weeks after osteotomy. Six weeks after surgery, micro-CT and mechanical testing were performed. Micro-CT analysis at four weeks after surgery showed that the intramedullary fracture callus in the TiNbSn alloy group had more bone volume and numerous bridging structures compared to the CP-Ti group (CP-Ti vs. TiNbSn alloy,  $34.3 \pm 13.1 \text{ mm}^3$  vs.  $61.3 \pm 19.6 \text{ mm}^3$ ,  $p = 0.02$ ; mean  $\pm$  standard deviation). At four weeks post-osteotomy, the healed tibia showed significantly higher strength in the TiNbSn alloy group compared with CP-Ti (CP-Ti vs. TiNbSn alloy,  $81.3 \pm 31.2 \text{ N}$  vs.  $133.7 \pm 46.6 \text{ N}$ ,  $p = 0.04$ ). TiNbSn alloy locking plates had a more positive impact on bone formation and bone strength restoration than the CP-Ti locking plates during the early phase of bone healing.

**Keywords:** locking plate; low Young's modulus; osteosynthesis; osteotomy; TiNbSn alloy

Tohoku J. Exp. Med., 2023 November, 261 (3), 199-209.

doi: 10.1620/tjem.2023.J075

## Introduction

Young's moduli of Ti6Al4V alloy and CP-Ti are 117 GPa and 107 GPa, respectively, lower than that of stainless steel (205 GPa) (Long and Rack 1998; Zhan et al. 2020). However, those are much higher than human cortical bone (11-20 GPa) (Bayraktar et al. 2004). The divergence of Young's moduli between the materials of the prosthesis and cortical bone causes stress shielding by inhibiting the load-sharing from the biomedical material to the bone (Glassman et al. 2006). Fracture treatment devices with excessive stiffness reportedly produce poor outcomes, including the delay and failure of bone healing (Henderson et al. 2011; Ebraheim et al. 2013). In contrast, previous studies have

shown that, on image assessment of fracture healing, intramedullary nails with titanium alloy of a low Young's modulus promoted fracture healing and bone strength restoration (Sha et al. 2009; Niinomi and Nakai 2011).

A new beta TiNbSn alloy having a low Young's modulus of less than 50 GPa has been developed to resolve the stress shielding (Matsumoto et al. 2005). The tensile strength of TiNbSn alloy is equivalent to that of Ti6Al4V alloy. When inserted into the rabbit femoral bone marrow cavity, TiNbSn alloy also showed excellent biocompatibility, comparable to that of the Ti6Al4V alloy. The cell culture tests observed reduced cytotoxic properties (Miura et al. 2011; Shiraiishi et al. 2020). Previous studies have also reported good corrosion resistance of TiNbSn alloys (Zheng

Received August 6, 2023; revised and accepted September 2, 2023; J-STAGE Advance online publication September 14, 2023

Correspondence: Yu Mori, Department of Orthopaedic Surgery, Tohoku University Graduate School of Medicine, 1-1 Seiryomachi, Aoba-ku, Sendai, Miyagi 980-8574, Japan.

e-mail: yu-mori@med.tohoku.ac.jp

©2023 Tohoku University Medical Press. This is an open-access article distributed under the terms of the Creative Commons Attribution-NonCommercial-NoDerivatives 4.0 International License (CC-BY-NC-ND 4.0). Anyone may download, reuse, copy, reprint, or distribute the article without modifications or adaptations for non-profit purposes if they cite the original authors and source properly. <https://creativecommons.org/licenses/by-nc-nd/4.0/>

et al. 2006; Rosalbino et al. 2012). The anodized TiNbSn alloy prepared in acetic acid and sulfuric acid electrolytes had high hydroxyapatite formation ability, strong bone bonding, and excellent osseointegration (Tanaka et al. 2016; Masahashi et al. 2017, 2019; Kunii et al. 2019; Mori et al. 2022a, b). The anodized TiNbSn alloy in the electrolytes of sodium tartrate demonstrated high photocatalytic activity and antimicrobial properties under ultraviolet light irradiation (Masahashi et al. 2021, 2023; Kurishima et al. 2022; Mori et al. 2023). By annealing above 423 K, TiNbSn alloy gradually increased the stiffness and Young's modulus, demonstrating that it is a functionally graded material (Hanada et al. 2014). The results of models of rabbit and murine tibia fractures treated with intramedullary nails indicated that the nails of TiNbSn alloy were more promoting osteosynthesis than other materials with high Young's Moduli (Fujisawa et al. 2018; Kogure et al. 2019; Mori et al. 2021). Furthermore, the effect of low Young's modulus of the fracture plate on osteosynthesis was assessed. Radiological, histological, and mechanical assessments indicated the superior effects of the TiNbSn alloy on bone-repairing behaviors in comparison with the Ti6Al4V alloy (Ito et al. 2022).

The present study aimed to determine the effect of the locking plate with low Young's modulus on osteosynthesis. A limitation of the previous study was that the stresses may have been distributed between the screw and plate because the screw and plate were not locked together in the conventional plate, which may have been insufficient to evaluate the effect of low Young's modulus TiNbSn alloy for fracture healing (Ito et al. 2022). The locking plate was designed to improve stability and reduce bone-plates compression (Bottlang et al. 2016). Additionally, biological bridge plating helps maintain a blood supply, enabling the functional reduction of complex fractures (Tsai et al. 2015). The impacts of TiNbSn alloy and CP-Ti locking plates on bone healing were investigated under conditions of no stress distribution between screw and plate. We examine whether the superiority of the bone healing-promoting effect shown by the TiNbSn alloy conventional plate can also be demonstrated by the TiNbSn alloy locking plate.

## Materials and Methods

### *Fabrication of TiNbSn alloy plate*

Fracture treatment plates with a screw-locking system made of TiNbSn alloy and CP-Ti were used in the present

study (Fig. 1). The 8-hole CP-Ti locking plate for middle phalanx fractures was commercially available (2.0/2.3 TriLock plate, Medartis, Basel, Switzerland). The preparation of a TiNbSn alloy has been described (Hanada et al. 2013). The composition of the TiNbSn alloy ingot was Ti-33.6%Nb-4%Sn (at. %). The TiNbSn alloy plates were produced from bars through an extrusion and swaging processes and fabricated using the same design as the CP-Ti (Ito et al. 2022). A commercially available screw made of Ti6Al4V alloy was applied in both groups (2.0 TriLock screw, Medartis). The free resonance vibration method measured Young's moduli of the plates (Hanada et al. 2014); TiNbSn alloy and CP-Ti plates had values of 49.1 GPa and 107 GPa, respectively. Microstructure observation of the surface of plates before and after use was performed using a laser microscope (VKX150, Keyence, Osaka, Japan) (Fujisawa et al. 2018).

### *Animals*

Male Japanese white rabbits were purchased from Japan SLC (Shizuoka, Japan) and housed in an environmentally controlled, pathogen-free animal facility at the animal unit of our institute. All experiments were conducted using approximately 18-week-old rabbits weighing between 2.8 and 3.4 kg. The rabbits were caged in individually. A total of 42 rabbits were used in this study. The animal experimental protocol was reviewed and approved by the animal studies committee of Tohoku University (protocol #2020-MdA-141-01).

### *Surgical procedure*

The surgical procedures were described previously (Ito et al. 2022). The rabbits were administered anesthesia through a combination of inhalation of 5% sevoflurane, intramuscular injection of ketamine at a dosage of 15 mg/kg, and intravenous injection of xylazine at a dosage of 2 mg/kg. Before surgery, cefazolin (30 mg/kg) was administered intravenously. The plate was placed to be centered directly below the tibia and fibula junction. Three proximal and three distal screws were placed to secure the plate. After the installation of the plate, we performed the osteotomy using a wire saw with a 1-mm width just below the junction. A standard transverse tibial osteotomy model with a 1 mm gap was created using this technique. After the surgery, the rabbits were permitted to walk freely and bear their full weight.

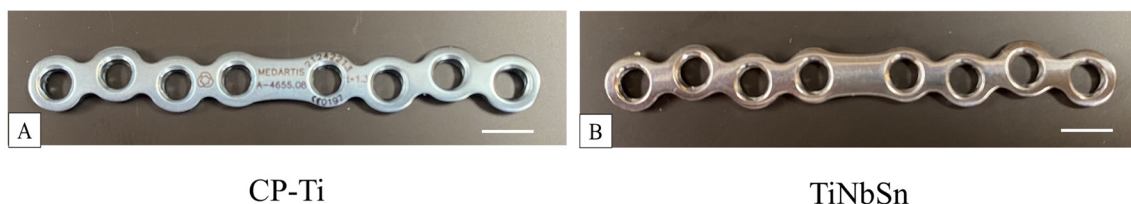


Fig. 1. Photographs of commercially pure titanium (CP-Ti) and TiNbSn alloy locking plates. (A) A plate made with CP-Ti. (B) A plate made with TiNbSn alloy. Scale bars indicate 5 mm.

### *Micro-computed tomography (micro-CT)*

To evaluate the bone healing process, radiographs, and micro-CT images were taken using a micro-CT scanner (LaTheta LCT-200; Hitachi Aloka Medical, Tokyo, Japan) at 4 and 6 weeks postoperatively ( $n = 6$  in each group). Scanning was performed over a 20 mm area centered on the osteotomy site. As previously described, twelve sagittal images were obtained every 15° using the DICOM viewer software (ZioCube, Ziosoft, Tokyo, Japan) (Kogure et al. 2019; Ito et al. 2022). The calculation of the volume of callus ( $\text{mm}^3$ ) was performed at 4 and 6 weeks after osteotomy. CT values greater than 1,000 Hounsfield Unit (HU) were determined to be a callus, and those greater than 1,500 HU were the original cortical bone following a previous report (Ito et al. 2022). The total and intramedullary callus area in each cross-section was measured using Image J version 1.53e (National Institutes of Health, Bethesda, MD, USA). For the calculation of the volume of these areas, measured values were then integrated.

Radial multiplanar reconstructed images were used to conduct a quantitative evaluation of bone bridging at 4 and 6 weeks post-surgery. Following previous studies, twelve longitudinal images were used to evaluate the opposite side in the plate attachment, and the measured total callus bridge width was calculated (CBW; mm) (Kogure et al. 2019). A schematic model of the CBW measurement is shown (Fig. 2A-C).

### *Histomorphometric analysis*

Histomorphometric analysis was performed four weeks postoperatively. The demineralized specimens were examined ( $n = 6$  in each group). The fixation was performed in a 10% neutral buffered formalin solution for three days. For eight weeks, demineralization was performed using 10% ethylenediaminetetraacetic acid and tetrasodium solution. 5-micrometer-thick sections were prepared and stained with hematoxylin, eosin, and Alcian blue. The newly formed bone and cartilage tissue in the callus was measured using a digital microscope camera (microscope: BX51, Olympus, Tokyo, Japan; digital camera: DP73, Olympus) (Kamimura et al. 2015; Izumiyama et al. 2019). Image J software measured the newly formed bone and cartilage ( $\text{mm}^2$ ) area (Baba et al. 2020).

Non-demineralized specimens were also examined four weeks postoperatively, and qualitative parameter measurement was performed using a previously described method ( $n = 3$  for each group) (Tanaka et al. 2016). Briefly, 7 and 2 days before euthanization, 10 mg/kg calcein (Dojindo Laboratories, Kumamoto, Japan) was injected and labeled on the tibia. The tibia was immediately fixed in 70% ethanol and soaked in Villanueva's bone staining reagent. Embedment of the samples was conducted with methyl methacrylate (Fujifilm Wako Chemicals, Tokyo, Japan). Non-demineralized cross-sections of 200- $\mu\text{m}$  thickness were obtained. Plastic slides with mounted cross sections were polished by a precision lapping machine

(Maruto, Tokyo, Japan). Histomorphometry was performed using a semi-automated image analysis system (System Supply, Ina, Japan), as previously described (Tanaka et al. 2016; Kunii et al. 2019).

### *Immunohistochemistry for osteocalcin*

The method of osteocalcin immunostaining has been previously reported (Oizumi et al. 2021; Hamada et al. 2022). First, an anti-osteocalcin antibody (M041, Anti-Bovine Osteocalcin, Takara Bio Inc., Shiga, Japan) was applied at a dilution of 1:1,000 and incubated at 4°C overnight. Next, the secondary antibody reaction was carried out with Histophane Simple Stain MAX-PO (Nichirei Bioscience, Tokyo, Japan) at room temperature for 40 minutes. Finally, 3,3'-diaminobenzidine tetrahydrochloride coloration (Sigma-Aldrich, St. Louis, MO, USA) was conducted for 3 minutes, and counterstaining was performed with hematoxylin. The measurements of osteocalcin-positive cells were conducted ( $\text{cells}/\text{mm}^2$ ) (Ito et al. 2022).

### *Mechanical test*

The bone strength of the repaired tibia was assessed at 4 and 6 weeks using a three-point bending test performed with a mechanical testing machine (Model 5566; Instron Corp., Norwood, MA, USA) (Kogure et al. 2019; Ito et al. 2022). Each group consisted of 6 samples. The tibia was loaded in the anterior-posterior direction. The spacing between the fulcrums was set at 4 cm. The test was conducted with the bending speed set at 2 mm/min until the specimen failed. The maximum load (N) was recorded, and the stiffness (N/mm) was estimated as the inclination of the liner part of the load-deflection curve.

### *Statistical analyses*

All data are expressed as the mean  $\pm$  standard deviation (SD). JMP software version 16 (SAS, Cary, NC, USA) was used for the statistical analyses. The statistical significance of the differences in values was determined using Student's t-test. A significance level of  $p < 0.05$  was considered statistically significant. The descriptive statistics for comparing bone parameters in non-demineralized specimens were conducted because of the small number of samples.

## **Results**

### *Radiographs*

Representative radiographic images are shown in Fig. 3. The radiographs were taken in the anteroposterior direction without the removal of plates. Callus formed four weeks postoperatively. In the TiNbSn alloy group, the osteotomy gap was filled, whereas in the CP-Ti group, the gap remained unfilled (Fig. 3A, B). Six weeks postoperatively, the bone repair was completed in both groups (Fig. 3C, D). There were no cases of fracture union failure.

Surface analysis of TiNbSn alloy plates

Laser microscopic images of TiNbSn alloy before and after implantation in rabbits are shown. Linear structures can be observed on the surface of the plate before use, but after four weeks of *in vivo* placement, bone formation occurred on the surface of the specimen, and no linear structures can be observed (Supplementary Fig. S1). No obvious structural changes suggesting corrosion were demonstrated.

Micro-CT analysis

Representative micro-CT images at 4 and 6 weeks

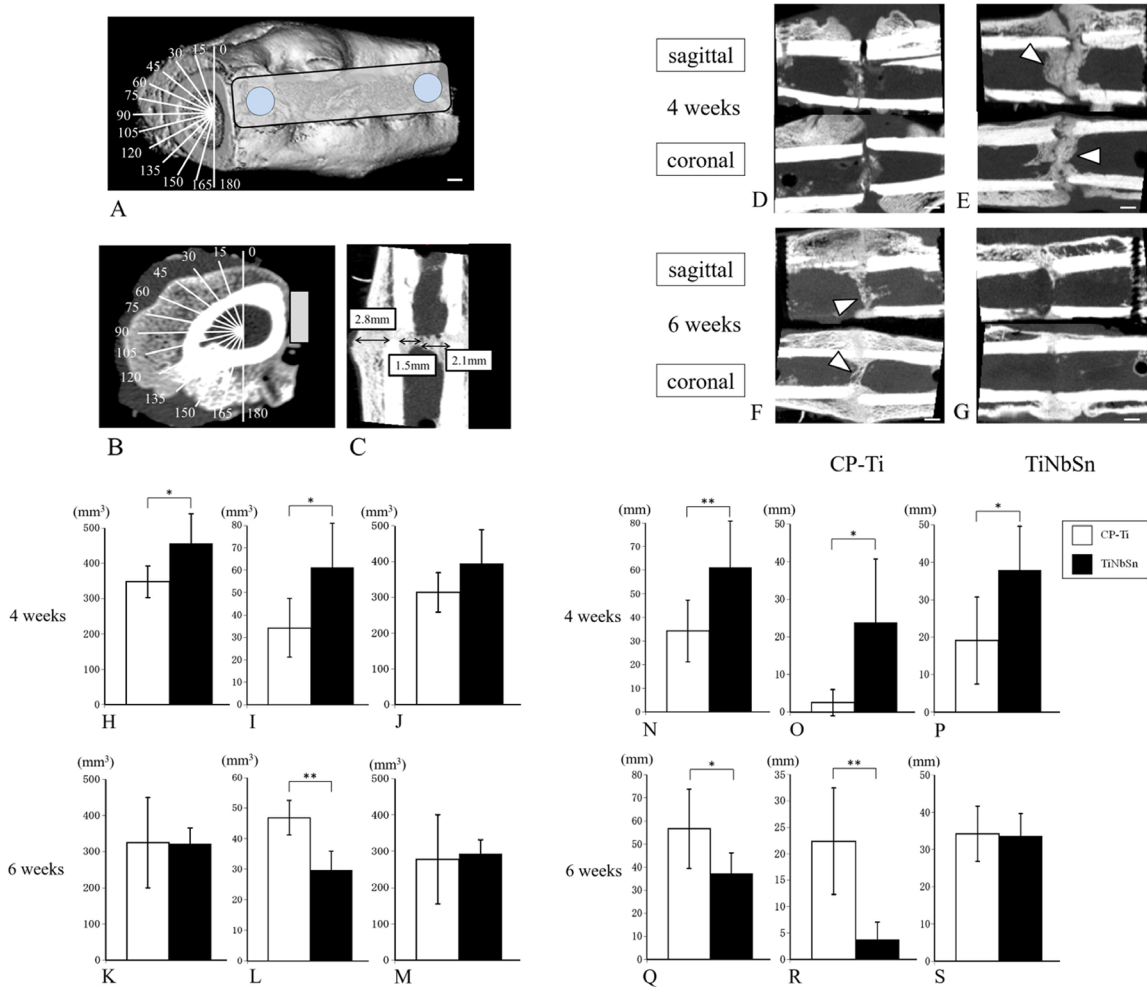


Fig. 2. Micro-computed tomography (micro-CT) analyses of new bone formation and callus bridge width (CBW). (A, B) Schematic models of CBW are shown. Twelve longitudinal cross-sectional images were used to evaluate the opposite side of the plate placement, and the sum of the measured callus bridge widths was defined as CBW (mm). The plate's schema is illustrated. (C) Example of measurement. The calculation of CBW: 2.8 + 1.5 + 2.1 = 6.4 mm. Scale bar indicates 2 mm. (D-G) Representative micro-CT images at 4 and 6 weeks after osteotomy. (D) Commercially pure titanium (CP-Ti), four weeks after osteotomy; (E) TiNbSn alloy, four weeks after osteotomy; (F) CP-Ti, six weeks after osteotomy; (G) TiNbSn alloy, six weeks after osteotomy. Sagittal and coronal reconstruction images are shown. Arrowheads indicate intramedullary bridging callus. Scale bar indicates 2 mm. (H-M) Micro-CT analyses of the new bone formation in the callus. (H), (I) and (J) are measurements at four weeks postoperatively; (H) total callus; (I) intramedullary callus; (J) extracortical callus. (K), (L) and (M) are measurements at six weeks postoperatively; (K) total callus; (L) intramedullary callus; (M) extracortical callus. (N-S) Micro-CT analyses of CBW width. (N), (O) and (P) are assessments at four weeks postoperatively; (N) total callus; (O) intramedullary callus; (P) extracortical callus. (Q), (R) and (S) are assessments at six weeks postoperatively; (Q) total callus; (R) intramedullary callus; (S) extracortical callus. Results are expressed as the mean ± SD (n = 6). \*p < 0.05, \*\*p < 0.01 using Student's t-test.

after osteotomy, significant differences were observed in total and intramedullary calluses in the TiNbSn alloy group than in the CP-Ti group (Total callus: CP-Ti vs. TiNbSn alloy,  $348.3 \pm 44.6 \text{ mm}^3$  vs.  $455.9 \pm 84.6 \text{ mm}^3$ ;  $p = 0.02$ ; Intramedullary callus: CP-Ti vs. TiNbSn alloy,  $34.3 \pm 13.1 \text{ mm}^3$  vs.  $61.3 \pm 19.6 \text{ mm}^3$ ;  $p = 0.02$ ) (Fig. 2H, I). No difference was observed in the extracortical region volume (Fig. 2J). At six weeks postoperatively, the callus volume had reduced compared to four weeks in both groups, indicating bone remodeling in the callus. At the six-week following the osteotomy, no significant difference in total callus volume was observed between the two groups (Fig. 2K). However, the more significant formation of the intramedullary callus was observed in the CP-Ti group than in the TiNbSn alloy group (CP-Ti vs. TiNbSn,  $46.9 \pm 5.7 \text{ mm}^3$  vs.  $29.6 \pm 6.4 \text{ mm}^3$ ;  $p < 0.001$ ) (Fig. 2L). No difference was observed in the extracortical callus volume (Fig. 2M).

The CBW values measured at 4 and 6 weeks after osteotomy are shown in Fig. 2N-S. At four weeks after osteotomy, the total intramedullary and extracortical CBW were significantly higher in the TiNbSn alloy group than in the CP-Ti alloy group (Total CBW: CP-Ti vs. TiNbSn,  $20.6 \pm 10.3 \text{ mm}$  vs.  $61.9 \pm 11.9 \text{ mm}$ ,  $p < 0.001$ ; Intramedullary CBW: CP-Ti vs. TiNbSn,  $2.5 \pm 3.5 \text{ mm}$  vs.  $23.8 \pm 16.9 \text{ mm}$ ,  $p = 0.01$ ; Extracortical CBW: CP-Ti vs. TiNbSn,  $19.1 \pm 11.6 \text{ mm}$  vs.  $37.9 \pm 11.8 \text{ mm}$ ,  $p = 0.02$ ) (Fig. 2N-P). At six weeks postoperatively, the CBW in the TiNbSn alloy group was further reduced in comparison with that at four weeks postoperatively, which reflected remodeling of the callus to mature cortical bone; in contrast, the CBW in the CP-Ti group had increased at this time point. The CBW values of total and intramedullary callus were significantly higher in the CP-Ti group than in the TiNbSn alloy group (Total CBW: CP-Ti vs. TiNbSn,  $56.6 \pm 17.1 \text{ mm}$  vs.  $37.3 \pm 8.9 \text{ mm}$ ,  $p = 0.03$ ; Intramedullary CBW: CP-Ti vs. TiNbSn,  $22.4 \pm 10.1 \text{ mm}$  vs.  $3.72 \pm 3.4 \text{ mm}$ ,  $p = 0.002$ ) (Fig. 2Q, R). The CBW values of extracortical callus were comparable in both groups (Fig. 2S).

#### Histomorphometric analyses

Representative images of the demineralized specimens

with hematoxylin and eosin stains are shown in Fig. 4A-D. At four weeks after osteotomy, new bone formation area in the total and intramedullary callus was significantly greater in the TiNbSn alloy group than CP-Ti group (total callus: CP-Ti vs. TiNbSn,  $19.3 \pm 4.8 \text{ mm}^2$  vs.  $28.8 \pm 7.7 \text{ mm}^2$ ,  $p = 0.03$ ; intramedullary callus: CP-Ti vs. TiNbSn,  $3.3 \pm 4.0 \text{ mm}^2$  vs.  $9.7 \pm 5.6 \text{ mm}^2$ ,  $p = 0.04$ ); however, no significant differences were found in the extracortical callus volume between the groups (Fig. 4E-G). In addition, there was a substantial difference in the new bone formation at the osteotomy site on the side of the plate installation in the TiNbSn alloy group (CP-Ti vs. TiNbSn,  $0.2 \pm 0.2 \text{ mm}^2$  vs.  $1.4 \pm 1.3 \text{ mm}^2$ ,  $p = 0.048$ ) (Fig. 4H).

In the assessment of the residual cartilage tissue in the callus at four weeks after osteotomy, the area of the residual cartilage was significantly higher in the CP-Ti group than in the TiNbSn alloy group (CP-Ti vs. TiNbSn,  $5.9 \pm 4.2 \text{ mm}^2$  vs.  $0.8 \pm 0.6 \text{ mm}^2$ ,  $p = 0.01$ ) (Fig. 5A-C).

Representative images of the non-demineralized specimens are shown (Fig. 6A-D). In the TiNbSn alloy group, bridging structures at the fracture site were observed both intramedullary and extracortical callus, while in the CP-Ti group, no bridging structures between bone fragments at the fracture site were observed. The results of the histological analyses demonstrated that the TiNbSn alloy group had a greater volume of new bone in the extracortical area compared to that observed in the CP-Ti group [median (interquartile range) CP-Ti vs. TiNbSn:  $13.5 \text{ mm}^2$  (5.8) vs.  $25.6 \text{ mm}^2$  (8.2)] (Fig. 6E, F).

#### Immunohistochemistry

Representative images of immunostaining for osteocalcin at four weeks post-osteotomy are shown in Fig. 7. The TiNbSn alloy group specimens had a more significant number of osteocalcin-positive osteoblasts than that of the CP-Ti group (Fig. 7A-D). Either in the extracortical and intramedullary callus, the quantitative assessment revealed a significantly more significant number of osteocalcin-positive cells in the TiNbSn alloy group than in the CP-Ti group (total callus: CP-Ti vs. TiNbSn,  $1,054 \pm 207 \text{ cells/mm}^2$  vs.  $1,626 \pm 317 \text{ cells/mm}^2$ ,  $p = 0.004$ ; intramedullary callus:

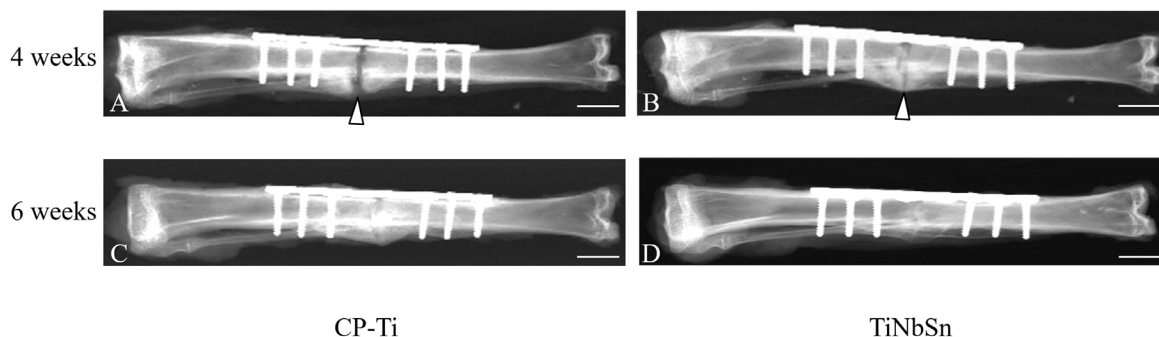


Fig. 3. Representative radiographs at 4 and 6 weeks after osteotomy.

(A) Commercially pure titanium (CP-Ti), four weeks after osteotomy; (B) TiNbSn alloy, four weeks after osteotomy; (C) CP-Ti, six weeks after osteotomy; (D) TiNbSn alloy, six weeks after osteotomy. Scale bar indicates 10 mm.

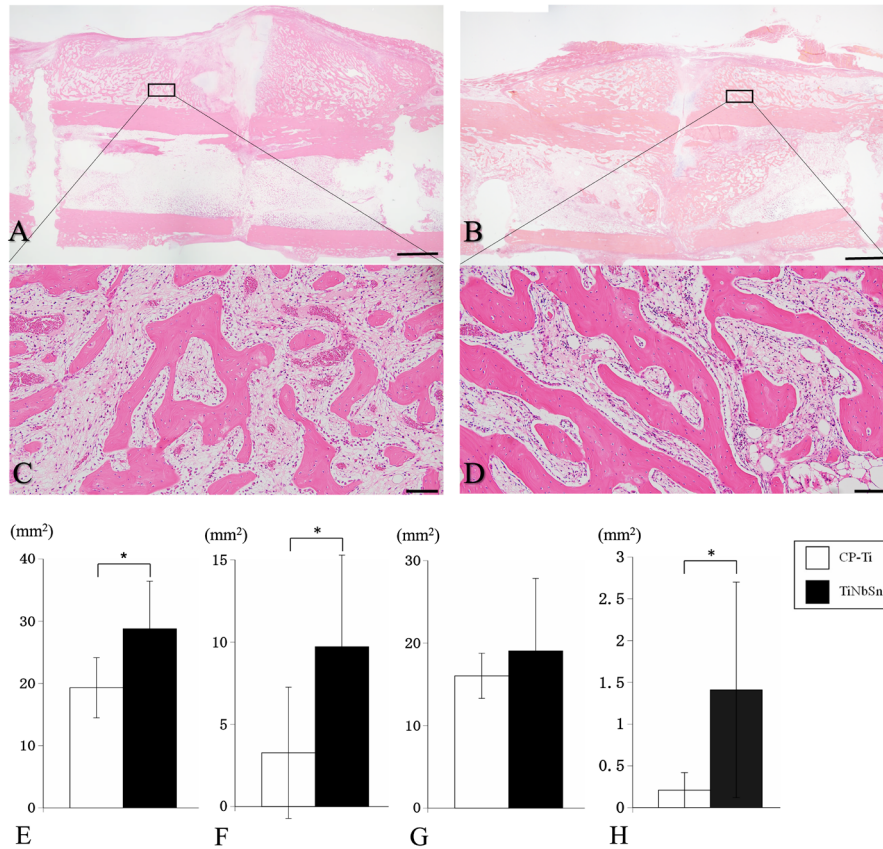


Fig. 4. Histomorphometric analyses of demineralized specimen.

Representative 4 × magnification images of the commercially pure titanium (CP-Ti) group (A) and the TiNbSn alloy group (B). The scale bar indicates 2 mm. Representative 10 × magnification images of the CP-Ti group (C) and the TiNbSn alloy group (D). Scale bar indicates 200 μm. Measurements of the new bone formation area; (E) total callus; (F) intramedullary callus; (G) extracortical callus; (H) osteotomy site on the side of the plate installation. Results are expressed as the mean ± SD (n = 6). \*p < 0.05 using Student's t-test.

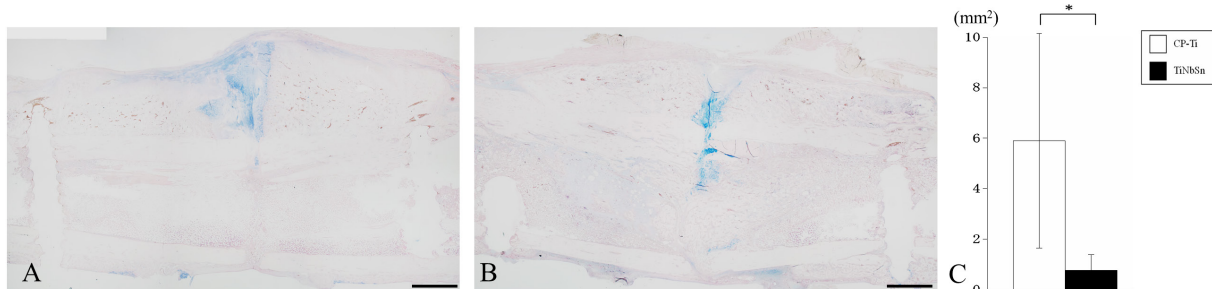


Fig. 5. Histomorphometric analyses of residual cartilage area.

Representative 4 × magnification image images of the commercially pure titanium (CP-Ti) group (A) and the TiNbSn alloy group (B). The scale bar indicates 2 mm. Quantitative analysis of the residual cartilage area (C). Results are expressed as the mean ± SD (n = 6). \*p < 0.05 using Student's t-test.

CP-Ti vs. TiNbSn,  $548 \pm 100$  cells/mm<sup>2</sup> vs.  $790 \pm 142$  cells/mm<sup>2</sup>,  $p = 0.007$ ; extracortical callus: CP-Ti vs. TiNbSn,  $506 \pm 116$  cells/mm<sup>2</sup> vs.  $836 \pm 178$  cells/mm<sup>2</sup>,  $p = 0.003$  (Fig. 7E-G).

#### Mechanical test

The results of the three-point bending test at 4 and 6 weeks are shown in Fig. 8. The maximum load and stiff-

ness of healed bone four weeks postoperatively were significantly higher in the TiNbSn alloy group than in the CP-Ti group (maximum load: CP-Ti vs. TiNbSn,  $81.3 \pm 31.2$  N vs.  $134 \pm 46.6$  N,  $p = 0.04$ ; Stiffness: CP-Ti vs. TiNbSn,  $68.2 \pm 45.2$  N/mm vs.  $168 \pm 41.9$  N/mm,  $p = 0.003$ ) (Fig. 8A, B). The TiNbSn alloy group demonstrated a significantly higher maximum load at the six-week postoperatively compared to the CP-Ti group (CP-Ti vs. TiNbSn,  $229 \pm 96.5$  N vs.  $351 \pm$

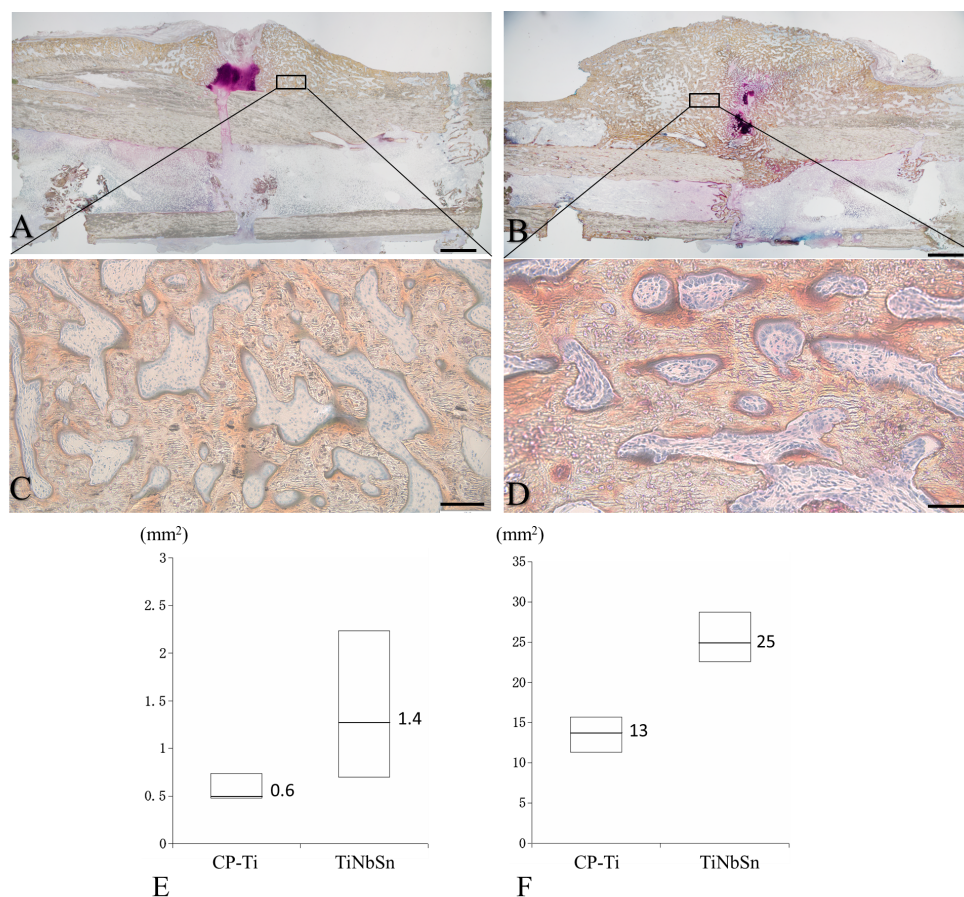


Fig. 6. Histomorphometric analyses of non-demineralized specimen.

There was more newly formed bone in the TiNbSn alloy group than in the the commercially pure titanium (CP-Ti) group, and the orientation of the formed laminar bone matched that of the tibia, indicating more advanced remodeling. (A) CP-Ti; (B) TiNbSn alloy at 4 × magnification (scale bar indicates 2 mm); (C) CP-Ti; (D) TiNbSn alloy at 20 × magnification (scale bar indicates 100 μm). Measurements of new bone formation in (E) intramedullary callus and (F) extracortical callus. The results are expressed as the median and interquartile range (n = 3).

81.1 N,  $p = 0.04$ ). No difference was found in the stiffness at six weeks after osteotomy (Fig. 8C, D).

### Discussion

This is the first report to demonstrate the effect of a locking plate made of a low Young's modulus titanium alloy in promoting bone healing. The results of this study indicated that treatment using the TiNbSn alloy locking plate led to faster bone healing and higher bone strength at four weeks after osteotomy compared to those observed with the CP-Ti locking plate. At the 4-week postoperative CT and histological analyses, the amount of intramedullary callus formation and CBW were higher in the TiNbSn alloy than in the CP-Ti group, suggesting that greater bone strength was achieved in the TiNbSn group due to the promotion of bridging structures within the intramedullary callus. Furthermore, the between-group difference in healed bone strength was significantly higher in the TiNbSn group at six weeks postoperatively. Optimization of load-sharing in the TiNbSn group suggested that the strength of healed

bone was also improved.

Although studies on the promotion of bone healing after fracture using TiNbSn alloy have been conducted previously (Fujisawa et al. 2018; Kogure et al. 2019; Mori et al. 2021), extracortical callus formation was mainly evaluated using a simple intramedullary nail model, and there were problems in the fixation, such as those associated with control of rotation, in these previous studies. In this study, we could precisely evaluate fracture healing due to plate fixation with a locking structure; it also allowed for the evaluation of the mechanism of fracture repair in the intramedullary callus. The presence of osteoblasts and osteoblastic precursor cells in the periosteum and endosteum has been confirmed (Mori et al. 2016). In this study, no difference was found in the extracortical callus formation between the TiNbSn alloy and CP-Ti groups; however, a significant difference was observed in the intramedullary callus formation in the early stages of fracture healing between the two groups. The recovery of bone strength in the TiNbSn alloy group was attributed to the accelerated

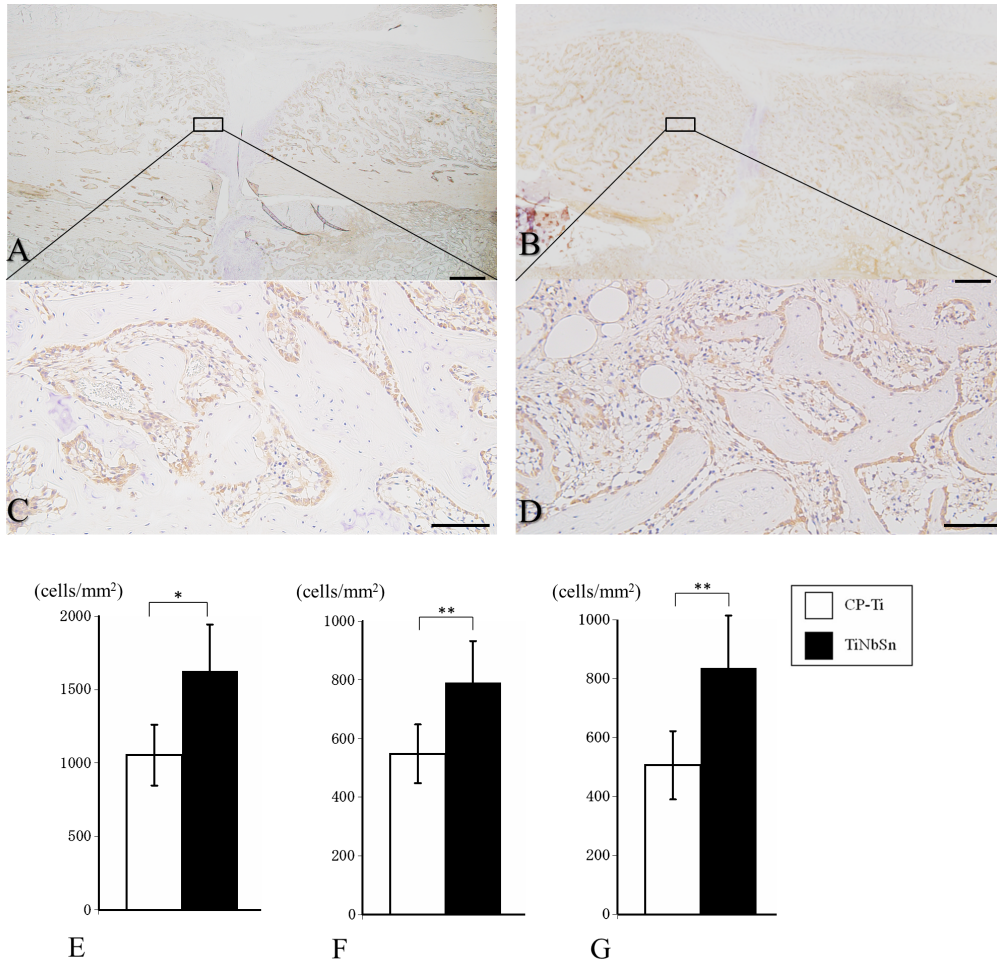


Fig. 7. Analyses of immunohistochemistry for osteocalcin expression. (A) Commercially pure titanium (CP-Ti); (B) TiNbSn alloy; 10 × magnification, scale bar indicates 500 μm. (C) CP-Ti, higher magnification; (D) TiNbSn alloy, higher magnification; 20 × magnification, scale bar indicates 100 μm. (E-G) Quantitative analyses of osteocalcin-positive cells; (E) total callus; (F) intramedullary callus; (G) extracortical callus. Results are expressed as the mean ± SD (n = 6). \*p < 0.05, \*\*p < 0.01 using Student's t-test.

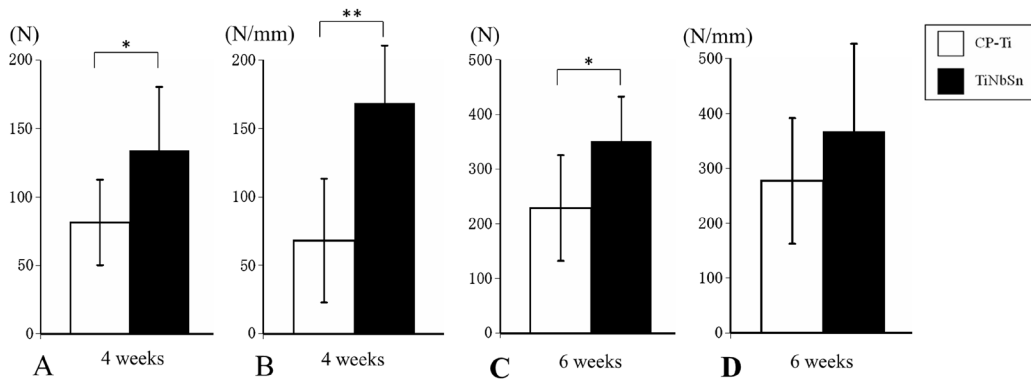


Fig. 8. Analyses of bone strength by mechanical testing in commercially pure titanium (CP-Ti) and TiNbSn alloy. (A) Maximum load, four weeks after osteotomy; (B) stiffness; 4 weeks after osteotomy; (C) maximum load; 6 weeks after osteotomy; (D) stiffness; 6 weeks after osteotomy. Results are expressed as the mean ± SD (n = 6). \*p < 0.05, \*\*p < 0.01 using Student's t-test.

formation of the intramedullary callus. In a rabbit tibial osteotomy model using conventional TiNbSn alloy plates, we reported that the TiNbSn alloy group promoted callus formation in the medullary cavity, resulting in early bone healing (Ito et al. 2022). The results of this study show similar findings in a rabbit tibial osteotomy model using TiNbSn alloy conventional plates. The study using conventional plates of TiNbSn alloy showed that bone fusion was complete at 8 weeks (Ito et al. 2022). The strength of healed bone at 6 weeks in the present study with the locking plates was equivalent to that at 8 weeks postoperatively in the study with the conventional TiNbSn alloy plates, suggesting that the locking plate system was able to promote more bone healing. Even at six weeks, there was a significant difference in the strength of the healed bone between the two groups, and the intramedullary and extracortical calluses were resorbed and replaced by mature bone. The callus volume and CBW in the TiNbSn alloy group were further reduced at six weeks than at four weeks postoperatively, which paradoxically resulted in them being lower than those of the CP-Ti group. We believe this reversal resulted from callus resorption and remodeling being more prevalent in the TiNbSn alloy group. The repair mechanism in the late stage of fracture healing was consistent with previous reports using intramedullary TiNbSn alloy nails (Fujisawa et al. 2018; Kogure et al. 2019; Mori et al. 2021).

The excessive stiffness of the plate might impair callus formation and bone healing (Henschel et al. 2017). In the present study, we believe that the accelerated callus formation in the bone defect on the site of plate installation in the TiNbSn alloy plate group was due to the appropriate load-sharing caused by the low Young's modulus of the TiNbSn alloy. Fracture treatment plates using Ti29Nb13Ta4.6Zr alloy with a low Young's modulus showed a tendency to promote osteosynthesis, although no quantitative evaluation was performed (Sumitomo et al. 2008; Niinomi and Nakai 2011). These findings were consistent with those of the present study.

The clinical applications of TiNbSn alloys have been discussed. In a previous study where a load-sharing analysis of a TiNbSn alloy stem was conducted using finite element methods, TiNbSn alloy stem was observed to improve load-sharing in the cortical bone and address the load-stress imbalance between the cortical bone and prosthesis stems (Yamako et al. 2017). A TiNbSn alloy stem for a hip prosthesis was developed (Hanada et al. 2014), and the results of the clinical trial demonstrated that TiNbSn alloy stems improved stress shielding, including thigh pain and loosening of the hip prosthesis (Chiba et al. 2021; Baba et al. 2023). Because TiNbSn alloy has achieved safety, durability, and material availability, future research should aim to use the TiNbSn alloy in fracture treatment devices clinically and to shorten the fracture treatment period.

As for the limitations of this study, this study was conducted in rabbits and is a preclinical study. Developing a TiNbSn alloy locking plate for human subjects will require

further studies in larger animals to determine the superiority of its osteogenesis-promoting effect and the risk of plate failure. Although the CP-Ti locking plates were used in this study as a control, a comparison of Ti6Al4V alloy locking plates and TiNbSn alloy locking plates with similar strength would be ideal in assessing the risk of fracture in large animals.

In conclusion, this study showed that the TiNbSn alloy locking plate was more effective for bone healing and strength than the CP-Ti locking plate four weeks after osteotomy, suggesting that the TiNbSn alloy plate promoted faster bone healing. Furthermore, the bone fracture strength of the fused bone was significantly higher in the TiNbSn group at six weeks, suggesting that bone strength was improved by optimizing load-sharing even after bone healing.

### Acknowledgments

This study was supported by the Japan Society for the Promotion of Science (No. 18K09052 to Yu Mori; No. 20H02458 to Naoya Masahashi).

### Author Contributions

Koguchi M., Mori Y., Kamimura M., Ito K., Tanaka H., Kurishima H., Koyama T., Mori N., Masahashi N., and Aizawa T. contributed substantially to the research design, the acquisition, analysis, and interpretation of data. All authors contributed to drafting the paper or revising it critically. All authors have read and approved the final submitted manuscript.

### Conflict of Interest

The authors declare no conflict of interest.

### References

- Baba, K., Mori, Y., Chiba, D., Kuwahara, Y., Kurishima, H., Tanaka, H., Kogure, A., Kamimura, M., Yamada, N., Ohtsu, S., Oyama, M., Masahashi, N., Hanada, S., Itoi, E. & Aizawa, T. (2023) TiNbSn stems with gradient changes of Young's modulus and stiffness reduce stress shielding compared to the standard fit-and-fill stems. *Eur. J. Med. Res.*, **28**, 214.
- Baba, K., Shiwaku, Y., Hamai, R., Mori, Y., Anada, T., Tsuchiya, K., Oizumi, I., Miyatake, N., Itoi, E. & Suzuki, O. (2020) Chemical stability-sensitive osteoconductive performance of octacalcium phosphate bone substitute in an ovariectomized rat tibia defect. *ACS Appl. Bio Mater.*, **3**, 1444-1458.
- Bayraktar, H.H., Morgan, E.F., Niebur, G.L., Morris, G.E., Wong, E.K. & Keaveny, T.M. (2004) Comparison of the elastic and yield properties of human femoral trabecular and cortical bone tissue. *J. Biomech.*, **37**, 27-35.
- Bottlang, M., Tsai, S., Bliven, E.K., von Rechenberg, B., Klein, K., Augat, P., Henschel, J., Fitzpatrick, D.C. & Madey, S.M. (2016) Dynamic stabilization with active locking plates delivers faster, stronger, and more symmetric fracture-healing. *J. Bone Joint Surg. Am.*, **98**, 466-474.
- Chiba, D., Yamada, N., Mori, Y., Oyama, M., Ohtsu, S., Kuwahara, Y., Baba, K., Tanaka, H., Aizawa, T., Hanada, S. & Itoi, E. (2021) Mid-term results of a new femoral prosthesis using Ti-Nb-Sn alloy with low Young's modulus. *BMC Musculoskelet. Disord.*, **22**, 987.
- Ebraheim, N.A., Martin, A., Sochacki, K.R. & Liu, J. (2013) Nonunion of distal femoral fractures: a systematic review.

- Orthop. Surg.*, **5**, 46-50.
- Fujisawa, H., Mori, Y., Kogure, A., Tanaka, H., Kamimura, M., Masahashi, N., Hanada, S. & Itoi, E. (2018) Effects of intramedullary nails composed of a new beta-type Ti-Nb-Sn alloy with low Young's modulus on fracture healing in mouse tibiae. *J. Biomed. Mater. Res. B Appl. Biomater.*, **106**, 2841-2848.
- Glassman, A.H., Bobyn, J.D. & Tanzer, M. (2006) New femoral designs: do they influence stress shielding? *Clin. Orthop. Relat. Res.*, **453**, 64-74.
- Hamada, S., Mori, Y., Shiwaku, Y., Hamai, R., Tsuchiya, K., Baba, K., Oizumi, I., Kanabuchi, R., Miyatake, N., Aizawa, T. & Suzuki, O. (2022) Octacalcium Phosphate/Gelatin Composite (OCP/Gel) enhances bone repair in a critical-sized transcortical femoral defect rat model. *Clin. Orthop. Relat. Res.*, **480**, 2043-2055.
- Hanada, S., Masahashi, N. & Jung, T. (2013) Effect of stress-induced  $\alpha'$  martensite on Young's modulus of  $\beta$  Ti-33.6Nb-4Sn alloy. *Mater. Sci. Eng. A*, **588**, 403-410.
- Hanada, S., Masahashi, N., Jung, T.K., Yamada, N., Yamako, G. & Itoi, E. (2014) Fabrication of a high-performance hip prosthetic stem using beta Ti-33.6Nb-4Sn. *J. Mech. Behav. Biomed. Mater.*, **30**, 140-149.
- Henderson, C.E., Kuhl, L.L., Fitzpatrick, D.C. & Marsh, J.L. (2011) Locking plates for distal femur fractures: is there a problem with fracture healing? *J. Orthop. Trauma*, **25** Suppl 1, S8-14.
- Henschel, J., Tsai, S., Fitzpatrick, D.C., Marsh, J.L., Madey, S.M. & Bottlang, M. (2017) Comparison of 4 methods for dynamization of locking plates: differences in the amount and type of fracture motion. *J. Orthop. Trauma*, **31**, 531-537.
- Ito, K., Mori, Y., Kamimura, M., Koguchi, M., Kurishima, H., Koyama, T., Mori, N., Masahashi, N., Hanada, S., Itoi, E. & Aizawa, T. (2022) beta-type TiNbSn alloy plates with low Young modulus accelerates osteosynthesis in rabbit tibiae. *Clin. Orthop. Relat. Res.*, **480**, 1817-1832.
- Izumiyama, T., Mori, Y., Mori, S., Mori, N., Kodama, T. & Itoi, E. (2019) The effect of anti-IL-6 receptor antibody for the treatment of MCh-lpr/lpr-RA1 mice that spontaneously developed destructive arthritis and enthesitis. *BMC Musculoskelet. Disord.*, **20**, 286.
- Kamimura, M., Mori, Y., Sugahara-Tobinai, A., Takai, T. & Itoi, E. (2015) Impaired fracture healing caused by deficiency of the immunoreceptor adaptor protein DAP12. *PLoS One*, **10**, e0128210.
- Kogure, A., Mori, Y., Tanaka, H., Kamimura, M., Masahashi, N., Hanada, S. & Itoi, E. (2019) Effects of elastic intramedullary nails composed of low Young's modulus Ti-Nb-Sn alloy on healing of tibial osteotomies in rabbits. *J. Biomed. Mater. Res. B Appl. Biomater.*, **107**, 700-707.
- Kunii, T., Mori, Y., Tanaka, H., Kogure, A., Kamimura, M., Mori, N., Hanada, S., Masahashi, N. & Itoi, E. (2019) Improved osseointegration of a TiNbSn alloy with a low Young's modulus treated with anodic oxidation. *Sci. Rep.*, **9**, 13985.
- Kurishima, H., Mori, Y., Ishii, K., Inoue, H., Mokudai, T., Fujimori, S., Itoi, E., Hanada, S., Masahashi, N. & Aizawa, T. (2022) Antibacterial activity of an anodized TiNbSn alloy prepared in sodium tartrate electrolyte. *Front. Bioeng. Biotechnol.*, **10**, 883335.
- Long, M. & Rack, H.J. (1998) Titanium alloys in total joint replacement—a materials science perspective. *Biomaterials*, **19**, 1621-1639.
- Masahashi, N., Hatakeyama, M., Mori, Y., Kurishima, H., Inoue, H., Mokudai, T., Ohmura, K., Aizawa, T. & Hanada, S. (2023) Photoinduced properties of anodized Ti alloys for biomaterial applications. *Sci. Rep.*, **13**, 13916.
- Masahashi, N., Mori, Y., Kurishima, H., Inoue, H., Mokudai, T., Semboshi, S., Hatakeyama, M., Itoi, E. & Hanada, S. (2021) Photoactivity of an anodized biocompatible TiNbSn alloy prepared in sodium tartrate / hydrogen peroxide aqueous solution. *Appl. Surf. Sci.*, **543**, 148829.
- Masahashi, N., Mori, Y., Tanaka, H., Kogure, A., Inoue, H., Ohmura, K., Kodama, Y., Nishijima, M., Itoi, E. & Hanada, S. (2019) Bioactive TiNbSn alloy prepared by anodization in sulfuric acid electrolytes. *Mater. Sci. Eng. C Mater. Biol. Appl.*, **98**, 753-763.
- Masahashi, N., Mori, Y., Tanaka, H., Kogure, A., Inoue, H., Ohmura, K., Kodama, Y., Nishijima, M., Itoi, E. & Hanada, S. (2017) Study of bioactivity on a TiNbSn alloy surface. *Thin Solid Films*, **639**, 22-28.
- Matsumoto, H., Watanabe, S. & Hanada, S. (2005) Beta TiNbSn alloys with low Young's modulus and high strength. *Mater. Trans.*, **46**, 1070-1078.
- Miura, K., Yamada, N., Hanada, S., Jung, T.K. & Itoi, E. (2011) The bone tissue compatibility of a new Ti-Nb-Sn alloy with a low Young's modulus. *Acta Biomater.*, **7**, 2320-2326.
- Mori, Y., Adams, D., Hagiwara, Y., Yoshida, R., Kamimura, M., Itoi, E. & Rowe, D.W. (2016) Identification of a progenitor cell population destined to form fracture fibrocartilage callus in DICKKOPF-related protein 3-green fluorescent protein reporter mice. *J. Bone Miner. Metab.*, **34**, 606-614.
- Mori, Y., Fujimori, S., Kurishima, H., Inoue, H., Ishii, K., Kubota, M., Kawakami, K., Mori, N., Aizawa, T. & Masahashi, N. (2023) Antimicrobial properties of TiNbSn alloys anodized in a sulfuric acid electrolyte. *Materials (Basel)*, **16**, 1487.
- Mori, Y., Fujisawa, H., Kamimura, M., Kogure, A., Tanaka, H., Mori, N., Masahashi, N. & Aizawa, T. (2021) Acceleration of fracture healing in mouse tibiae using intramedullary nails composed of beta-type TiNbSn alloy with low Young's modulus. *Tohoku J. Exp. Med.*, **255**, 135-142.
- Mori, Y., Masahashi, N. & Aizawa, T. (2022a) A review of anodized TiNbSn alloys for improvement in layer quality and application to orthopedic implants. *Materials (Basel)*, **15**, 5116.
- Mori, Y., Mori, N. & Aizawa, T. (2022b) Improving osteoinductive properties and imparting antibacterial activity to titanium alloys. *J. Bone Miner. Metab.*, **40**, 720-721.
- Niinomi, M. & Nakai, M. (2011) Titanium-based biomaterials for preventing stress shielding between implant devices and bone. *Int. J. Biomater.*, **2011**, 836587.
- Oizumi, I., Hamai, R., Shiwaku, Y., Mori, Y., Anada, T., Baba, K., Miyatake, N., Hamada, S., Tsuchiya, K., Nishimura, S.N., Itoi, E. & Suzuki, O. (2021) Impact of simultaneous hydrolysis of OCP and PLGA on bone induction of a PLGA-OCP composite scaffold in a rat femoral defect. *Acta Biomater.*, **124**, 358-373.
- Rosalbino, F., Maccio, D., Scavino, G. & Saccone, A. (2012) In vitro corrosion behaviour of Ti-Nb-Sn shape memory alloys in Ringer's physiological solution. *J. Mater. Sci. Mater. Med.*, **23**, 865-871.
- Sha, M., Guo, Z., Fu, J., Li, J., Yuan, C.F., Shi, L. & Li, S.J. (2009) The effects of nail rigidity on fracture healing in rats with osteoporosis. *Acta Orthop.*, **80**, 135-138.
- Shiraishi, N., Masumoto, H., Takahashi, K., Tenkumo, T., Anada, T., Suzuki, O., Ogawa, T. & Sasaki, K. (2020) Histomorphometric assessments of peri-implant bone around Ti-Nb-Sn alloy implants with low Young's modulus. *Dent. Mater. J.*, **39**, 148-153.
- Sumitomo, N., Noritake, K., Hattori, T., Morikawa, K., Niwa, S., Sato, K. & Niinomi, M. (2008) Experiment study on fracture fixation with low rigidity titanium alloy: plate fixation of tibia fracture model in rabbit. *J. Mater. Sci. Mater. Med.*, **19**, 1581-1586.
- Tanaka, H., Mori, Y., Noro, A., Kogure, A., Kamimura, M., Yamada, N., Hanada, S., Masahashi, N. & Itoi, E. (2016) Apatite formation and biocompatibility of a low Young's modulus Ti-Nb-Sn alloy treated with anodic oxidation and hot water. *PLoS One*, **11**, e0150081.
- Tsai, S., Fitzpatrick, D.C., Madey, S.M. & Bottlang, M. (2015) Dynamic locking plates provide symmetric axial dynamization

- to stimulate fracture healing. *J. Orthop. Res.*, **33**, 1218-1225.
- Yamako, G., Janssen, D., Hanada, S., Anijs, T., Ochiai, K., Totorige, K., Chosa, E. & Verdonshot, N. (2017) Improving stress shielding following total hip arthroplasty by using a femoral stem made of beta type Ti-33.6Nb-4Sn with a Young's modulus gradation. *J. Biomech.*, **63**, 135-143.
- Zhan, X., Li, S., Cui, Y., Tao, A., Wang, C., Li, H., Zhang, L., Yu, H., Jiang, J. & Li, C. (2020) Comparison of the osteoblastic activity of low elastic modulus Ti-24Nb-4Zr-8Sn alloy and pure titanium modified by physical and chemical methods.

- Mater. Sci. Eng. C Mater. Biol. Appl.*, **113**, 111018.
- Zheng, Y., Wang, B.L., Wang, J.G., Lia, C. & Zhao, L.Z. (2006) Corrosion behaviour of Ti-Nb-Sn shape memory alloys in different simulated body solutions. *Mater. Sci. Eng. A Struct. Mater.*, **438**, 891-895.

### Supplementary Files

Please find supplementary file(s);  
<https://doi.org/10.1620/tjem.2023.J075>

---